Manuscripts on omics research for model bees I

Deliverable D9.11

February 2022

[1]*Philippe Bulet*, [2]*Karim Arafah*, [2]*Dalel Askri*, [2]*Sébastien Voisin*

[1]*CR UGA, IAB, InsermU1209, CNRS UMR5309*, [2]*Plateforme BioPark d'Archamps*

PoshBee

Pan-european assessment, monitoring, and mitigation of stressors on the health of bees

Prepared under contract from the European Commission

Grant agreement No. 773921
EU Horizon 2020 Research and Innovation action

Project acronym:	**PoshBee**
Project full title:	**Pan-european assessment, monitoring, and mitigation of stressors on the health of bees**
Start of the project:	June 2018
Duration:	60 months
Project coordinator:	Professor Mark Brown Royal Holloway, University of London www.poshbee.eu

Deliverable title:	Manuscripts on omics research for model bees I
Deliverable n°:	D9.11
Nature of the deliverable:	Report
Dissemination level:	Public
WP responsible:	WP9
Lead beneficiary:	BIOPARK, CNRS
Citation:	Bulet, P., Arafah, K., Askri, D., & Voisin, S. (2022). *Manuscripts on omics research for model bees I*. Deliverable D9.11 EU Horizon 2020 PoshBee Project, Grant agreement No. 773921.
Due date of deliverable:	Month n°45
Actual submission date:	Month n°45

Deliverable status:

Version	Status	Date	Author(s)
1.0	Final	February 2022	[1]Bulet P. [2]Arafah K., [2]Askri D., [2]Voisin S. [1]CNRS, [2]BIOP

Table of contents

Preface

The Western honey bee, *Apis mellifera*, is the most commonly managed pollinator of major crops, offering services and value to the ecosystem and to our economy. Honey bees are exposed to a variety of abiotic and biotic stressors that may represent constraints for sustainable agriculture. In order to decipher the molecular mechanisms involved in the cross talk between a stressor (biotic or abiotic) on its host and to estimate their molecular impact alone or in combination, a peptidomics/proteomics workflow based on mass spectrometry (MS) was initiated on *A. mellifera* (model bee I). Complementary MS approaches were combined to generate molecular knowledge related to the impact of stressors on honey bee health. As a first step Matrix-assisted laser desorption/ionization was chosen as this technique enables the generation of molecular mass fingerprint characteristics of tissues that may be impacted by the stressors of interest. Following this first omics, we introduced molecular cartography of the honey bee, referred to as MALDI imaging (MALDI IMS) for measurement of the spatial distribution of molecules in biological tissues of *A. mellifera* in response to a biotic stressor. In this manuscript, we:

- Produced representative molecular mass fingerprints of selected tissue collections obtained by dissection. This was followed by MALDI IMS workflow optimization including specimen embedding and positioning as well as washing and matrix application.
- Reported the use of MALDI IMS to follow the molecular impact of an experimental infection of *Apis mellifera* with the microsporidian *Nosema ceranae.*
- Observed a distinction in the molecular profiles between the two conditions recorded from different anatomical sections of the gut tissue.
- Visualised differences in the molecular profiles of the brain, thoracic ganglia, hypopharyngeal gland, and haemolymph.
- Introduced MALDI IMS as an effective approach to monitor the impact of *N. ceranae* infection on *A. mellifera*. This opens perspectives for the discovery of molecular changes in peptide/protein markers that could contribute to a better understanding of the impact of stressors and toxicity on different tissues of a bee in a single experiment.

Summary

Among pollinating insects, bees play a critical role in boosting reproduction of wild and commercial plants and thus contribute to the preservation of plant biodiversity and sustainability of food webs. In the last few decades, domesticated and wild bees have been subjected to biotic and abiotic threats causing various health disorders. In our manuscript, we focus on nosemosis, an infection caused by a single-cell microsporidian parasite *Nosema*, which chronically infects the digestive tract of honey bees. Therefore, developing solutions to improve bee health including nosemosis is increasingly necessary, but still lacking. Here, we focused our investigations on the development of an omics strategy referred to as MALDI molecular mass fingerprint (MALDI MFP) and its integration with MALDI imaging mass spectrometry (MALDI IMS) to monitor which tissues would be impacted in a comparison between *Nosema*-infected and non-infected Western honey bees (*Apis mellifera*) (**Figure 1**).

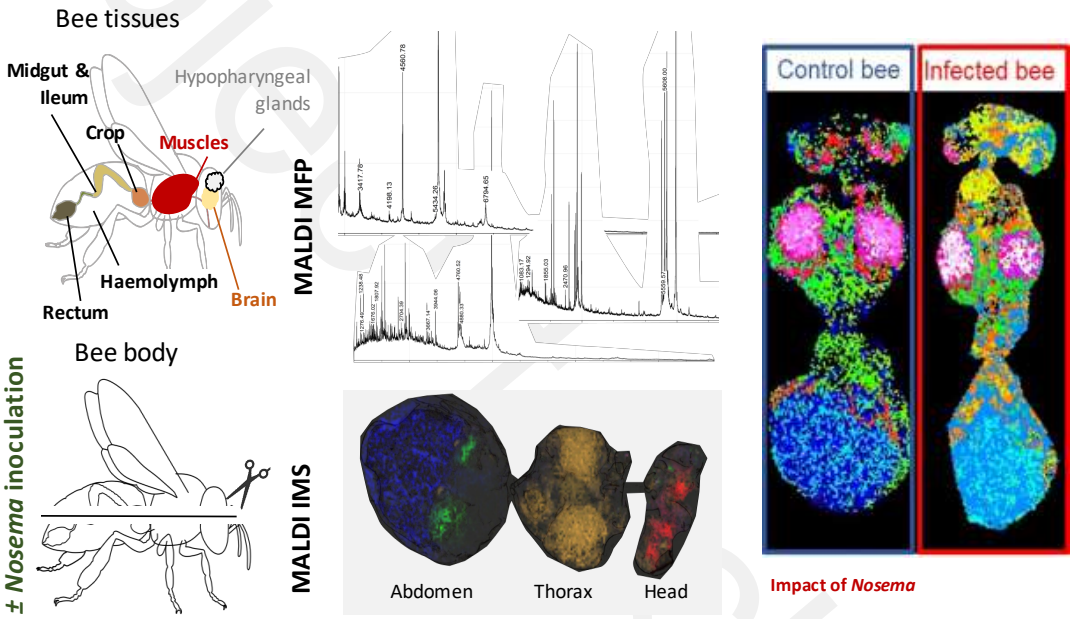

Figure 1: Summary of the omics strategy used to follow the impact of nosemosis on overall body sections of the honey bee *Apis mellifera*

1. Introduction

Over the past few decades, Matrix-assisted laser desorption/ionization imaging mass spectrometry (MALDI IMS) of tissues has gained popularity. MALDI IMS, historically developed by Caprioli and colleagues [1], is a label-free method that provides information on the spatial distribution of drugs and their metabolites [2], endogenous metabolites [3,4], biomarkers like lipids [5,6], glycolipids [7], and peptides/proteins [8–11], within sections of organs or whole-bodies/organisms [12–17]. In theory, this powerful tool can directly allow access, in a multiplex analysis, to hundreds or thousands of analytes in parallel on flash-frozen tissue sections [18] and on formalin fixed and paraffin embedded samples [19]. Due to this unique performance and its enhanced credibility, MALDI IMS has the power to facilitate mechanistic studies and discovery of potential molecular signatures of diseases for a deeper understanding of the pathologically related processes.

To date, MALDI IMS is commonly used in pharmaceutical research and industry to determine the importance of accumulation and metabolization of drugs in various tissues [2]. For example, MALDI IMS has been used to monitor the distribution of xenobiotic substances in skin [20,21] and artificial models of human epidermis [22]. Furthermore, MALDI IMS is also widely used in life sciences,

biomedical and pharmaceutical research and development on a multitude of biological matrices [23,24]. Advancements in MALDI IMS instrumentation for improved resolution and sensitivity, sample preparation workflows including innovative chemical strategies for on-tissue chemical derivatization or to generate novel matrices, and data management and processing, offer the ability to precisely quantify tissues molecular abundances at a high-resolution level [25–29]. MALDI IMS technology is now used for analyses of biological samples belonging to both plant [30–33] and animal kingdoms, including human specimens [23,34,35]. Given the increasing use of MALDI IMS on animal models, this approach was also investigated in different invertebrate models and for the first time in insects to map neuropeptides within the neuronal tissues of the cricket *Acheta domesticus* [36]. Subsequently, MALDI IMS was applied to bee models to follow the distribution of queen-signal compounds [37], analyze the neuropeptide distribution in the Africanized honey bee (*Apis mellifera*) brain [38,39] or to follow the degradation and toxicity of pesticides [40–42] and to identify the most abundant metabolites [43].

The European honey bee *A. mellifera* is the most managed pollinator in our agricultural systems and represents significant economic value [44,45]. The health of *A. mellifera* has been declining in many countries around the world, raising concerns about human food resources [46,47]. Among a series of possible factors contributing to colony losses, infectious diseases caused by parasites and pathogens are significant contributors in altering bee health [48,49]. Among them, nosemosis is one of the possible factors that negatively impacts honey bee health and especially the *A. mellifera* population worldwide [50,51]. The causative agents are unicellular microsporidian parasites, essentially *Nosema apis* and *N. ceranae* [52]. *Nosema* spores are ingested into the digestive tract of the host where they can develop and multiply intracellularly before being expelled in the faecal matter following destruction of epithelial cells [53]. *Nosema* disease affects colony performances and bee health by many processes [54]. The impact of *Nosema* disease at the individual level includes numerous physiological alterations, such as (i) metabolic changes [55,56], (ii) energy stress/management [56], (iii) pheromone and hormone production [57], (iv) inhibition of epithelial cells apoptosis [58], (v) immune function suppression [55,59,60], (vi) life span shortening [56,61,62], (vii) cognitive deficits [63,64], (viii) acceleration of transition to forager activities [65] and (ix) changes of gut microbiota [66]. We recently conducted a study with the aim to decipher the impact of a *per-os* inoculation of *A. mellifera* with spores of *Nosema* on the first off-gel proteomics on the different anatomical sections of the gut [67]. Upon oral infection, we observed at an early stage of the infection (four days) that midgut proteins were the most altered (50 down-regulated, 16 up-regulated) compared to the control experiment with most of them being involved in metabolic and oxidative phosphorylation pathways [67].

To pursue our investigations on the underlying molecular mechanisms, MALDI IMS was conducted on the entire body of *A. mellifera* in this context in order to follow and establish the first comprehensive spatial histo-proteomics picture of the impact of *Nosema* infection on whole bee sections. The aim of the present work was to propose an experimental workflow for the study of the impact of a stressor in bee tissues by MALDI IMS. Specifically, we combined two MALDI MS approaches, MALDI molecular mass fingerprints (MALDI MFP), and MALDI IMS to generate molecular tissue signatures (gut, thoracic muscles, brains, hypopharyngeal glands, and haemolymph) and histo-molecular images of honey bees infected with spores of *Nosema*. By combining these two MALDI approaches, we highlighted that *Nosema* did not exclusively impact the gut tissue, which is in agreement with our findings related to the molecular consequences of *Nosema* infection on the immune response, on the thoracic muscles and on the nervous system.

2. Tissue signatures by direct MALDI profiling experiment on honey bee organs

2.1. Materials

2.1.1. Biological materials

To provide material for the experimental studies, Buckfast adult bees were collected in a field apiary at the Plateforme BioPark d'Archamps (Archamps, France). The absence of *Nosema* infection was confirmed by microscopical observation of gut content. Emerging honey bees were placed in plastic cages (Ickowicz, France) and maintained in incubators at 33°C ± 1°C and 60% ±20% relative humidity.

2.1.2. Sample preparation for MALDI MFPs

To enable MALDI molecular mass fingerprinting (MFPs), thoracic muscles, brains and hypopharyngeal glands of honey bees were collected from six worker bees under a binocular Microscope. Brains and hypopharyngeal glands were dissected according to the procedure of Carreck et al. [68]. The collected tissues were rinsed in PBS and kept at -80°C until use. The digestive tract of 12 bees were individually dissected from one-day-old bees and segmented in three sections: the crop, the midgut and ileum, and the rectum. Gut tissues were washed in PBS and then placed in low protein binding tubes (LoBind, Eppendorf, France) containing 20µL of TFA 1% and vortexed. Haemolymph was collected according to the procedure published by Arafah et al. [69] in those 12 bees.

For MALDI MFPs spectra acquisition, brain, hypopharyngeal glands and muscles were supplemented with 10µL of TFA 1 %, crushed on a MALDI polished target plate (Bruker Daltonics, Germany) and covered by 1µL of TFA 1 %. Tissues were then covered with 1µL of a 10 mg/mL 4-HCCA matrix solution prepared in 70 % ACN with TFA 2.5 % acidified water (v:v). Gut sections were vortexed and 1µL of the suspension was laid on the MALDI polished target plate. After drying the droplet was covered with 1µL of a 15 mg/mL 4-HCCA solution prepared as above. MALDI MFPs spectra were recorded with an AutoFlex III – Smartbeam MALDI MS as described below. At the end of mass spectra acquisition, an average spectrum representative of each tissue was generated using the mMass software v5.5.0.

2.1.3. MALDI parameters

MALDI MFPs (mass range 600-18,000 Da) spectra were acquired in a positive ion linear mode using an AutoFlex™ III - Smartbeam MALDI mass spectrometer equipped with a 200 Hz 355-nm frequency-tripled Nd:YAG laser (Bruker Daltonics, Germany). The instrument was calibrated using a mixture of two sets of peptides (APISCAL) and proteins (ProtMix) covering the dynamic range of interest. The composition of the homemade APISCAL is the following: synthetic pure Apidaecin and Abaecin, two antimicrobial peptides from *A. mellifera* (average *m/z* of 2,109 and 3,879, respectively), synthetic pure melittin, the major venom component, (average *m/z* of 2,847); and ETD, a recombinant peptide, (average *m/z* of 4,839). ProtMix (Protein Calibration Standard I, Bruker Daltonics) is a manufacturer-available mixture of four peptides and proteins (Insulin, Ubiquitin, Cytochrome C and Myoglobin at average *m/z* of 5,734, 8,565, 12,360 and 16,952, respectively).

2.2. Results and Discussion

We identified potential features of six honey bee tissues (brain, hypopharyngeal glands, thoracic muscles, crop, midgut and ileum, and haemolymph) by generating their molecular mass fingerprints (MFPs) using MALDI mass spectrometry. This approach, which has been greatly improved over the past 20 years, has demonstrated its feasibility, robustness and cost-effectiveness in identifying a wide range of microorganisms (e.g. bacteria, mycobacteria and certain fungal pathogens [70], parasites [71,72] and more recently some microsporidian pathogens for honey bee [73]. We also used MALDI MFPs to monitor the impact of experimental microbial infections on honey bee haemolymph [69]. To create model MFPs, an average spectrum for each tissue was recorded as the most representative

histo-molecular signature of the tissues (**Figure 2**). From these average spectra, a total of 46 molecular-related ions in muscles, 51 in brain, 34 in hypopharyngeal glands, 20 in haemolymph, 34 in crop, 39 in midgut and ileum and 38 in rectum were recorded between *m/z* 1,000-14,000 (Figure 2 red numbers). Finally, 21 molecular-related ions in muscles, 23 in brain, 11 in hypopharyngeal glands, 4 in haemolymph, 8 in crop, 18 in midgut and ileum, and 15 in rectum were found specific for each tissue between the mass range considered (Figure 2 green numbers). The number of molecular-related ions was considerably reduced due to unavoidable cross contamination between some tissues and the haemolymph that infiltrates all tissues. Using MALDI MFPs, we obtained molecular mass signatures for the (i) brain, (ii) hypopharyngeal glands, (iii) thoracic muscles, (iv) haemolymph, and (iv) three anatomical sections of the gut tissue (crop, midgut-ileum and rectum) to serve their identification *in situ* by MALDI IMS.

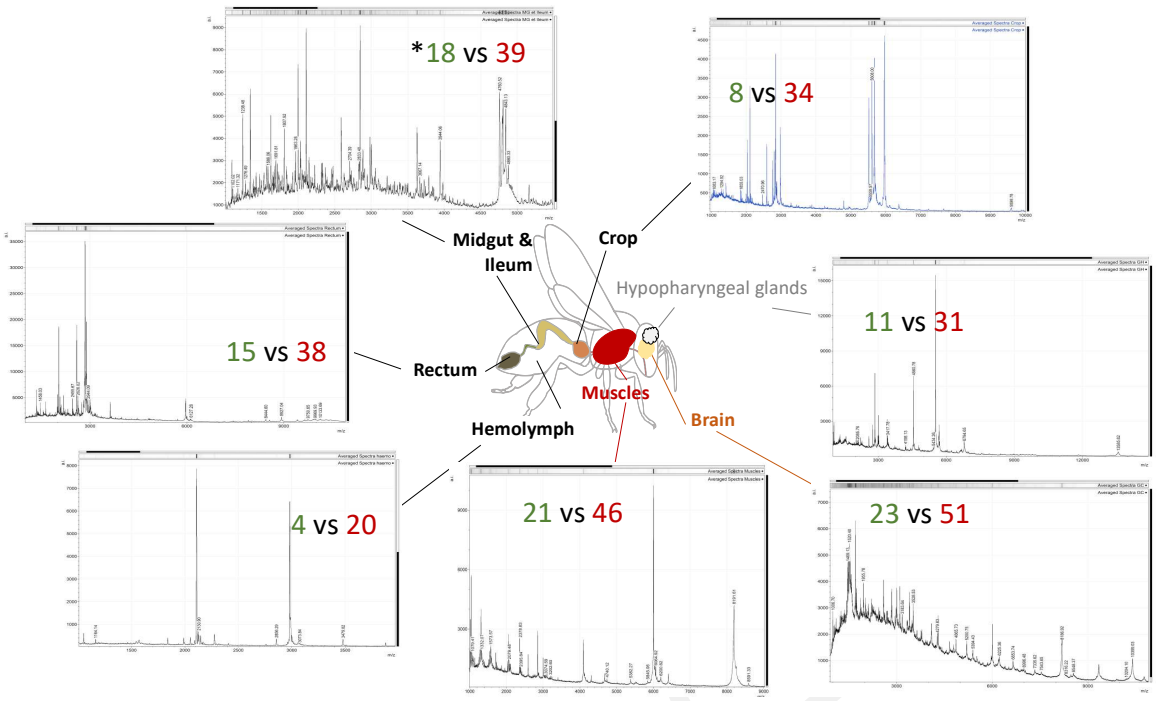

Figure 2: Representative spectra of each honey bee tissue analysed by MALDI-MS. From the average spectra, series of ions (numbers in red) were recorded for each tissue while the specific ions for each tissue are given in green. The mass spectra were recorded between m/z 1,000-14,000

3. Experimental workflow for MALDI IMS on the honey bee model: from tissue embedding to MALDI imaging

MALDI IMS was introduced less than 15 years ago and has since become an effective technique to investigate the biological and physiological functions in bees. For instance, *A. mellifera* brain neuropeptides were mapped in order to correlate aggressiveness and ontogeny with the obtained neuropeptide signatures [38,39]. More recently, Zhang and colleagues used MALDI IMS to evaluate the degradation and the toxicity of two neonicotinoid pesticides in honey bees through oral and contact exposures [74].

Tissue processing describes the steps required to take an animal or human tissue from fixation to the state where it is completely infiltrated with a suitable histological wax to embed it in preparation for cryo-section cutting on the microtome. In our study, we implemented a MALDI IMS protocol from honey bee preparation to whole-body scale imaging of the bee to investigate the molecular pattern changes in the context of nosemosis. The workflow (**Figure 3**) outlines the different steps involved in

preparing a fully infiltrated and embedded honey bee, ready to be cryo-sectioned on a cryomicrotome on different cutting planes.

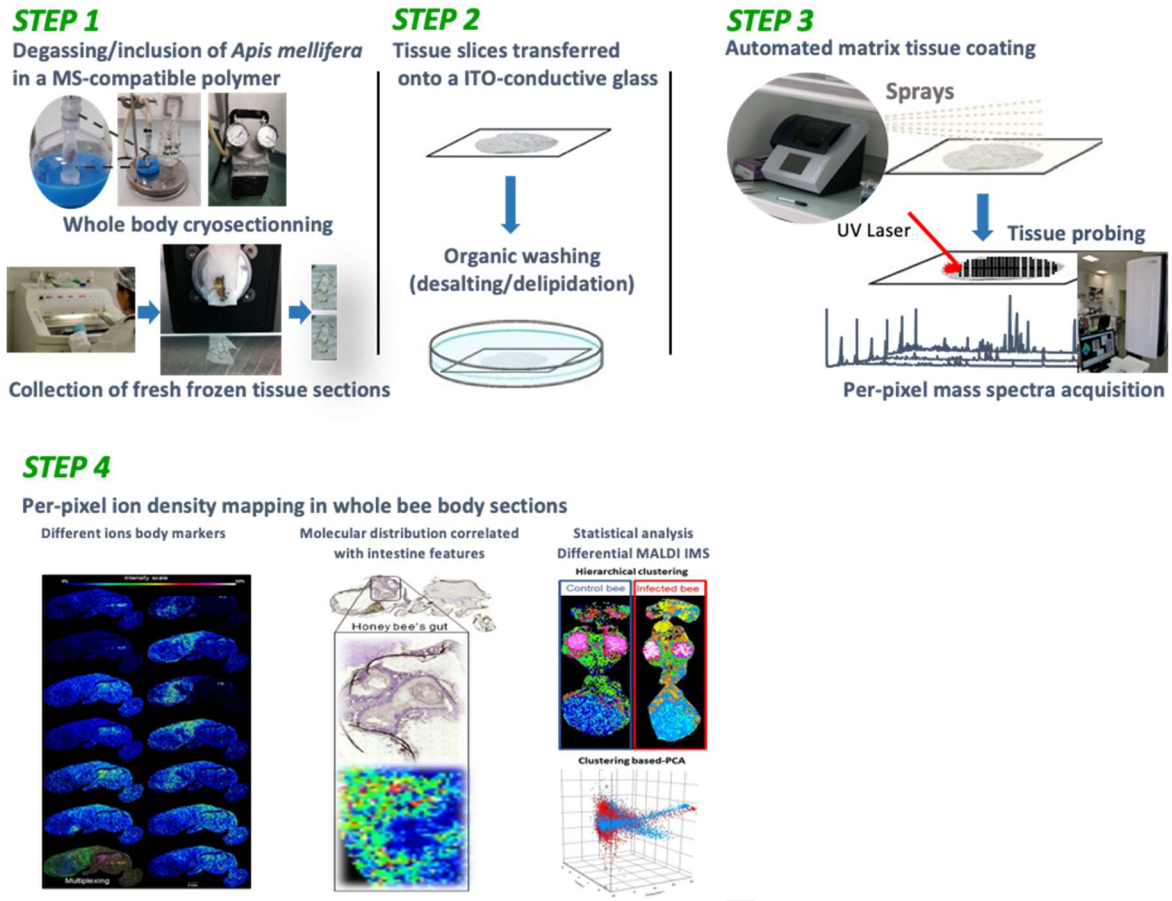

Figure 3: Whole-body MALDI IMS workflow applied to *Apis mellifera*

3.1. Materials

3.1.1. Biological materials

A brood frame was collected in June 2020 from one colony of Buckfast bees in a field apiary at the Plateforme BioPark d'Archamps (Archamps, France). Emerging honey bees were placed in plastic cages (Ickowicz, France) and maintained in incubators at 33°C ± 1°C and 60% ±20% relative humidity. The bees were fed syrup (InvertBee, Alp'Abeilles, France) *ad libitum*.

3.1.2. Sample preparation for MALDI IMS

To obtain histological blocks for MALDI IMS, honey bees were first anesthetized using carbon dioxide and individually embedded into a 2% (w:v) solution of low viscosity 90kDa carboxymethyl cellulose (CMC) polymer prepared in ultrapure water. Additionally, the embedded bees were instantaneously vented for 20 minutes under 600 mbar vacuum using a home-made device apparatus to ensure optimal bee bodies inclusion; the remaining air from the bees' respiratory system and from around their cuticle was thereby substituted with low viscosity CMC. The prepared bodies were then transferred into a filled tube with a chilled solution of the 250kDa CMC polymer. Once prepared, the samples were stored at -80°C for 24 hours before being sliced.

Before being sliced for MALDI IMS, the CMC-embedded body blocks were transferred from -80°C inside a cryomicrotome (Leica CM1950, Germany) maintained at -20°C and left to reach this appropriate cutting temperature for 15 minutes. A series of fresh frozen cryosections (15µm thickness) were performed and collected onto classical histological slides (Dominique Dutscher, France). Cryo-sections were stained for 20 seconds using hematoxylin. Serial sections were also collected and transferred onto conductive Indium Tin Oxide (ITO)-coated glass slides (Bruker Daltonics, Germany). Before processing, structural lipids present on the surface of the tissue sections were washed out by three baths in pure ethanol (only immersion followed by total drying of slice between each rinsing) and one bath in pure chloroform (a one-second immersion). The images of tissues were then digitized using the Nikon CoolScan 9000 (Nikon, Japan) for automated MALDI IMS process teaching and the Mirax high-resolution desktop microscope (Zeiss, Germany) for observations of histological features. The tissue sections were coated with a solution of DHB matrix by spraying with the ImagePrep nebulizer (Bruker Daltonics, Germany), using two runs of the method provided by the manufacturer (DHB_standard_1). **Table 1** summarizes a series of protocols that were tested to obtain an optimized proteomics spectrum. The best result was obtained with DHB matrix dissolved at 20mg/mL in equal volume of MetOH/Water acidified with 0.2 % TFA final concentration.

Table 1: Comparative protocols of sample preparation for MALDI imaging studies

Imaged Tissues	Section plane	Washing (# of iteration)	MALDI Matrix (mg/mL)	Solvant vol:vol	ImagePrep runs
Abdomen	Sagittal	Pure EtOH (4)	SA (15)	ACN 60% / TFA 0.2%	3
Abdomen	Sagittal	No wash	SA (15)	ACN 60% / TFA 0.2%	3 *versus* 4
Abdomen	Sagittal	70% EtOH 70 or 60% EtOH (1)	SA (15)	ACN 60% / TFA 0.2%	3
Abdomen	Sagittal	Pure CHCl3 vs pure EtOH (1)	SA (15)	ACN 60% / TFA 0.2%	3
Abdomen	Sagittal	Pure EtOH (1)	4HCCA (15)	ACN 70% / TFA 0.2%	3
Abdomen	Sagittal	EtOH (1) then 70% ACN (1)	4HCCA (15)	ACN 70% / TFA 0.2%	3
Whole body	CS ou CF	Pure EtOH 100 (4)	sDHB (10)	ACN 60% / TFA 0.2%	2
Abdomen	Sagittal	Pure EtOH 100 (4)	sDHB (10)	ACN 60% / TFA 0.2%	2
Head/Thorax junction	Frontal	Pure EtOH (2)	sDHB (10)	ACN 70% / TFA 0.2%	3
Head, thorax, abdomen	Frontal	Pure EtOH (3)	sDHB (15)	ACN 70% / TFA 0.2%	2 *versus* 3
Whole body then head, thorax, abdomen	Frontal	Pure EtOH (3) then CHCl3 (1)	DHB (15)	ACN 70% / TFA 0.2%	2
Body	Frontal	Pure EtOH (3) then CHCl3 (1)	DHB (20)	ACN 70% / TFA 0.2%	2
Body	Frontal	Pure EtOH (3) then CHCl3 (1)	DHB (20)	MeOH 50% / TFA 0.2%	2
Body	Frontal	Pure EtOH (3) then CHCl3 (1)	DHB (20)	MeOH 30% / TFA 0.2%	2
Body	Frontal	Pure EtOH (3) then CHCl3 (1)	DHB (20)	MeOH 50% / TFA 0.2%	2
Body	Frontal	Pure EtOH (3) then CHCl3 (1)	DHB (20)	MeOH 50% / TFA 0.2%	2
Body	Frontal	Pure EtOH (3) then CHCl3 (1)	DHB (20)	MeOH 50% / TFA 0.2%	2
Whole body then head, thorax, abdomen	Frontal	Pure EtOH (3) then CHCl3 (1)	DHB (20)	MeOH 50% / TFA 0.2%	2
Head, thorax, abdomen then whole body	Frontal	Pure EtOH (3) then CHCl3 (1)	DHB (20)	MeOH 50% / TFA 0.2%	2
Body	Frontal	Pure EtOH (3) then CHCl3 (1)	DHB (20)	MeOH 50% / TFA 0.2%	2

3.2. Results and Discussion

3.2.1. Inclusion and embedding optimization

Insects are protected by a stiff primary exoskeleton (cuticle), meaning that sectioning the whole insect is quite challenging compared to slicing individual organs or mammalian tissues. The first step of our experimental workflow was to include and embed the entire honey bee body under vacuum. To address this challenge, we focused on two successive solutions (low density for inclusion, medium viscosity for embedding) of a MALDI IMS compatible polymer, namely carboxymethyl cellulose (CMC; **Figure 4**). This two-step approach is critical to remove the air entrapped in all externally contacting anatomical structures including the tracheal sacs beneath the hard cuticle and to preserve the

anatomical structures during cryoslicing. To our knowledge, this is the first report on the use of a low viscosity CMC polymer solution to include and preserve histology in fresh frozen insect tissue sections. In their study, Pratavieira and colleagues seem not to embed the head but to apply an instantaneous head freezing step in nitrogen as described by Seeley and Caprioli [35,38,39] for mammal organs.

Following the inclusion, a 250kDa CMC polymer solution was preferred to the 90kDa polymer because of its higher viscosity as an embedding medium, thus producing a harder specimen block to slice. As reported in the literature, this type of embedding solution was previously recommended for tissue preparation for MALDI IMS analyses [75–77].

In their study, Zhang and collaborators mapped pesticides throughout the whole honey bees' body cryosections using the OCT (Optimal Cutting Temperature) polymer as the embedding medium [74]. However, in other works, this embedding polymer was considered as non-suitable for MALDI imaging of small molecules (below 1kDa) as it easily protonates and therefore contaminates MALDI mass spectra [78,79] and favours subsequent potential ion suppression [80,81]. To circumvent this drawback, Truong and colleagues eliminated the OCT polymer from the tissue surface using an ammonium buffer to perform MALDI imaging lipidomics [82].

3.2.2. Organ visualization using sagittal and frontal section axes

Visualizing the distribution of compounds (*e.g.* metabolites, lipids, peptides/proteins) among different organs of a honey bee may assist in responding to the impact of a stressor and in determining potential "molecular signatures" for specific organs. To obtain an exhaustive image of the impact of a stressor on *A. mellifera*, once included, the CMC embedded body blocks were cryosliced according to sagittal and frontal planes to image as many organs as possible that may be direct or indirect targets of the stressor(s) (*e.g.* infectious, pesticide). We initiated MALDI images of *A. mellifera* in a sagittal plane (for an example **see Fig.3, Step 4** pictures on the left).

Our results revealed that although we were able to get images of different body sections (head, thorax and abdomen) details remained difficult to obtain. For example, we did not observe clear images of the central nervous system and more importantly of the different anatomical sections of the gut tissue, which may represent the main target of our infection model, nosemosis. To overcome this problem, sections in a frontal plane were prepared, this plane being often considered to be the most suitable for studying the abdominal content and especially the midgut as this proximal part of the bee gut tract twists around the midgut, the Malpighian tubules and the ileum [68].

3.2.3. Pretreatment of the tissue sections and matrix selection

Following inclusion, embedding and slicing, we first tested a combination of solvents to delipidate and desalt the tissue sections, a depletion step deemed important to optimize peptide/protein detection [80,83]. In a second step, we evaluated the quality of recorded spectral signal from direct tissue imaging using SA, 4-HCCA, DHB (**Table 1**), the three most frequently matrices employed. To assess tissue complexity, we looked at the ionic signal recorded from body segments (head, thorax, abdomen) through targeted tissue imaging of region of interest (ROI) *versus* whole body sections (**Table 1**). To achieve this, 15µm of fresh frozen cryosections were prepared in sagittal and frontal planes, and ion peaks from the MALDI imaging spectra were extracted and compared. Their relative intensities were examined within the selected mass range of analysis (*m/z* 1,000-20,000) and with the lowest chemical background taken into account (data not shown). The best on-tissue imaging signal was obtained with DHB at 20 mg/mL prepared in a methanolic solution (**see Fig. 4**) following delipidation/desalting using a washing protocol based on three baths in pure ethanol and one bath in pure chloroform (each bath for one second). We tried various combinations of depletion and matrix, based on the few studies that existing on insects and specifically on bees. Pratavieira et al. (2014, 2018), selected a longer rinsed step and only with ethanol solutions and they applied a 4-HCCA matrix. At the beginning of our experiments, we also used the ethanol alone method but we rapidly observed

an improvement of spectra acquisition with addition of chloroform [38,39]. Concerning the matrix, they chose the HCCA, more appropriate for detection of small molecules, appropriate in their case because they worked in the mass range 700-4,000 Da. In our methodology, we proposed to cover samples with DHB to visualize ions in a larger mass range (mass range 1 kDa – 18 kDa).

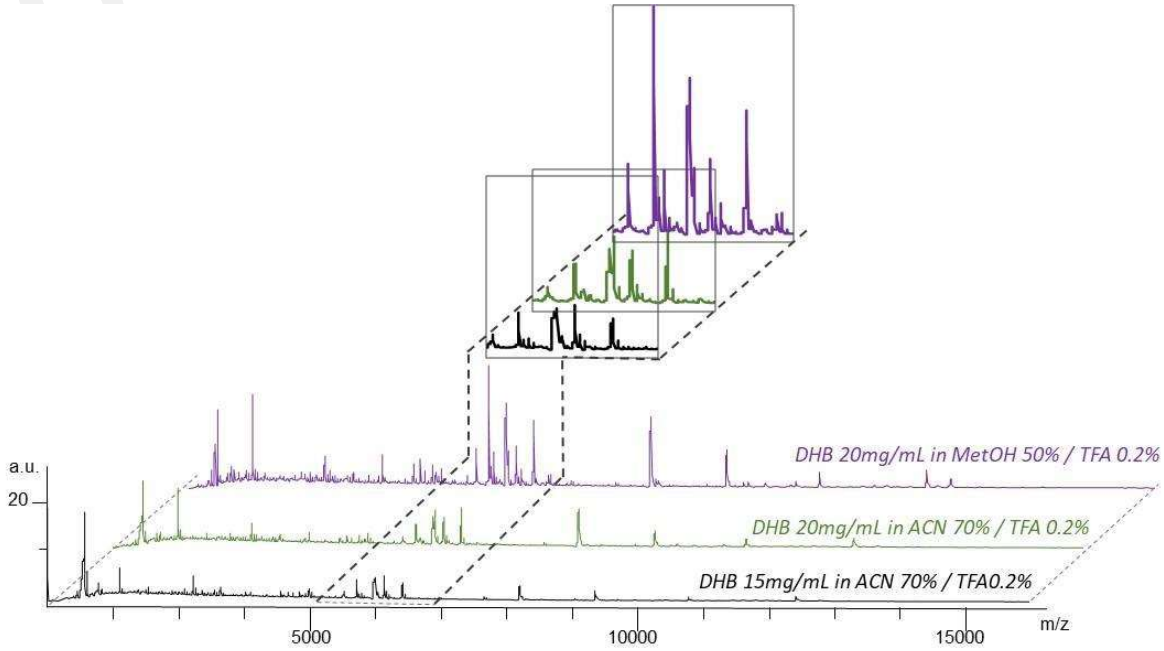

Figure 4: On tissue MALDI IMS signal comparison of three DHB-matrix preparations.

3.2.4. Honey bee histo-molecular atlas

After optimizing the sample preparation for MALDI IMS using frontal cryosections of the honey bee, we compared the lists of the molecular-related ions identified in each bee tissue's MFP with those imaged in the whole bee body. Considering a potential difference of 10 Da between the molecular-related ions recorded after MALDI MFP and those observed by MALDI IMS, one molecular-related ion marker was found to be representative for five (**Table 2**, highlighted masses in grey) of the seven tissues targeted in this study. In the molecular image (**Figure 5A**), we found four different molecular-related ion markers for the hypopharyngeal glands, the midgut combined to the ileum, the rectum, and the thoracic muscles including a *m/z* at 4,554, 4,834, 6,117 and 8,170, respectively. An additional molecular-related ion at *m/z* 1,842 was found as a signature of the crop in a MALDI image generated from another bee (**Figure 5B**). The crop is not consistently visible since it depends on whether the bee has just eaten (crop larger than the rectum) or not (rectum larger than the crop).

Table 2: Lists of peaks identified as potential molecular markers of honey bee tissues. All values are expressed in m/z. Peaks used as tissue markers for the MALDI imaging are underlined in grey. HG: Hypopharyngeal glands, MG: Midgut.

Muscles	Brain	HG*	Crop	MG-Ileum	Rectum	Hemolymph**
1079.41	1006.70	2085.76	1083.17	1102.02	1372.47	1164.14
1332.07	1469.13	2281.84	1294.92	1171.32	1388.51	2109.57
1573.57	1493.09	3417.78	1855.03	1238.48	1403.51	2130.90
1596.21	1520.40	3433.18	1893.92	1276.49	1456.03	2856.29
2079.48	1955.78	3449.38	2470.96	1529.17	2455.90	3479.82
2096.17	3183.64	4198.13	5559.57	1586.06	2626.02	5963.16
2357.00	3528.53	4560.78	5608.00	1676.02	2739.00	
2378.83	4279.63	5434.26	9598.78	1691.81	2944.09	
2395.84	4865.73	6669.66		1807.92	6127.28	
2419.04	5200.75	6794.65		1963.28	8444.60	
3033.49	5394.43	13585.62		2704.57	8927.04	
3074.59	6225.36	5520.76		2833.40	9750.65	
3202.60	6653.74			3667.14	9914.29	
3240.58	6784.05			3944.06	9969.93	
4740.12	6996.48			4760.52	10133.69	
5382.27	7335.62			4802.24		
5845.06	7543.65			4843.13		
6064.92	8186.92			4880.33		
6200.82	8316.22					
8191.61	8470.00					
8591.33	8548.37					
	10204.10					
	10399.03					

** for the hypopharyngeal glands, the molecular mass in red at 5520.76 is corresponding to Royalisin** for the haemolymph, the molecular masses in red at 2109.57 and 5963.16 are corresponding to the systemic immune peptides Apidaecin and to the* Apis mellifera *Chymotrypsin inhibitor (AMCI), respectively.*

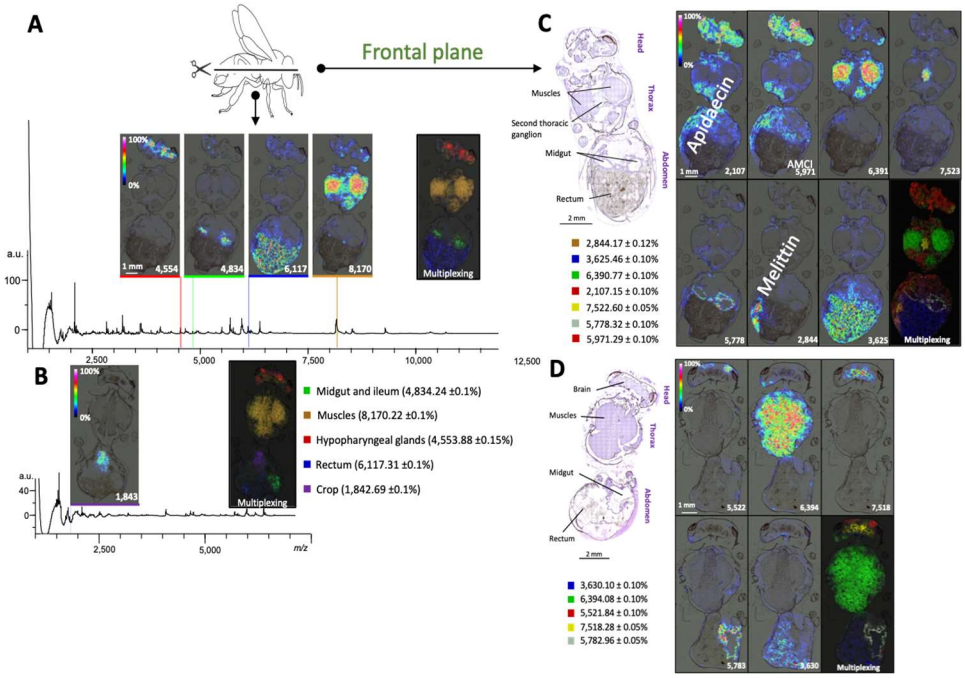

Figure 5: Molecular mass spectra and images of markers identified by MFPs extracted from MALDI IMS analyses of frontal whole-body sections of Apis mellifera (A,B). Molecular images of markers identifying bee tissues/organs (C,D).

For example, the rectum mostly represented the total abdomen content, while we cannot recognize the crop. Considering the haemolymph peak list, among the molecular-related ions identified, the ones corresponding to the immune peptide Apidaecin (2108.57 Da), and the *Apis mellifera* chymotrypsin inhibitor (AMCI, UniProtKB entry P56682, [84]; 5962.16 Da) were also recorded (**Table 2**, masses in red).

First, we imaged the haemolymph through Apidaecin (theoretical average *m/z* 2,109.44) and AMCI (theoretical *m/z* 5,963.81). A molecular-related ion at 2,107.15 (**Figure 5C**) is close to the theoretical average value of Apidaecin and a second one at *m/z* 5,971.29 is expected to correspond to AMCI, a serine-type endopeptidase inhibitor that we have structurally characterized (unpublished work, Plateforme BioPark d'Archamps, October 2020) and is known to be circulating in the haemolymph [84]. In a second step, complementary molecular-related ions (**Figure 5C,D**) specific to the second thoracic ganglion (*m/z* 7,523) and to the brain (*m/z* 7,518), muscles (*m/z* 6,391; *m/z* 6,394), midgut (*m/z* 5,778; *m/z* 5,782) harboring villosities, and rectum content (*m/z* 3,625; *m/z* 3,630) were evidenced. Interestingly, additional tissues were imaged through specific ions. In the abdomen, the venom gland was depicted through the molecular-related ion of Melittin at *m/z* 2,844 (**Figure 5C**), the major component of bee venom [85,86]. Within the abdomen, the two molecular-related ions at *m/z* 5,778 (Figure 4A) and 5,783 (**Figure 5D**) specifically imaged the midgut epithelium.

The combination of MALDI MFP and MALDI IMS used in this study allowed us to discriminate the midgut epithelium from the gut content (**Figure 6**). These results show the robustness of our MALDI IMS workflow to prevent molecular-related ion delocalization within tissues, and prompt us to apply our workflow to follow the direct impact of nosemosis on the gut tissue, the vertical flight muscles, the nervous system and the haemolymph.

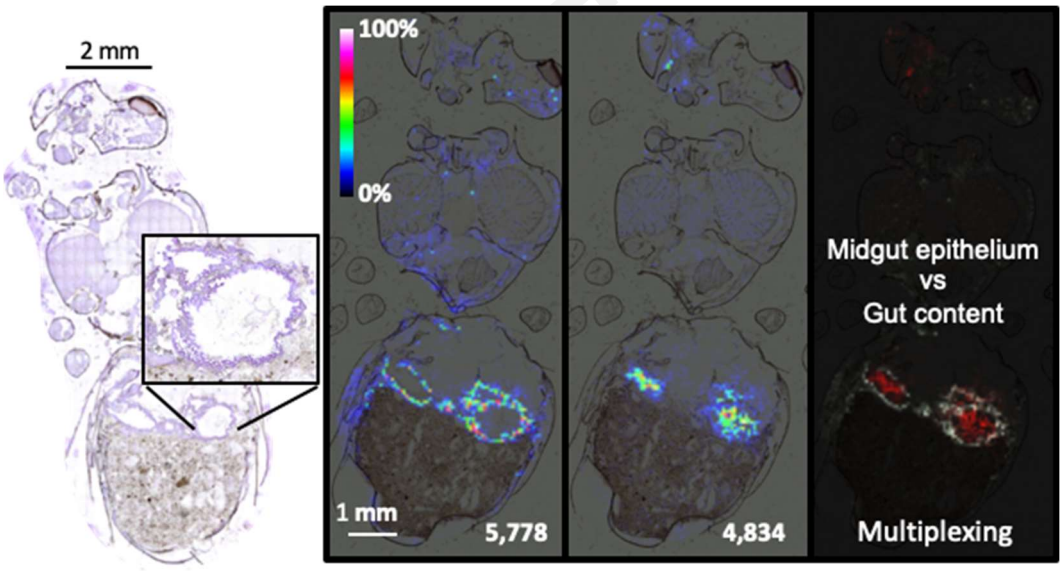

Figure 6: Molecular images of two markers of the midgut. The two markers of the midgut previously identified were observed and demonstrated a complementarity with the histological features between the midgut epithelium (*m/z* 5,778) and the midgut content (*m/z* 4,834). Intensity scale from 0 to 100% of the molecular-related ions.

4. Differential histo-proteomics changes in *Apis mellifera* following infection with *Nosema ceranae*

As part of this study, we experimentally infected honey bees with spores of *N. ceranae* and evaluated the consequences of this infection at the peptidomics/proteomics levels and for all body parts 16 days

after inoculation. Nosemosis is a globally prevalent disease in domestic honey bees and its effects are diverse, impacting the honey bee from the cellular to the behavioral level [54]. We hypothesized the existence of an alteration of the peptidomics/proteomics profiles of the gut but also of other organs.

4.1. Biological materials

A brood frame was collected in June 2020 from one colony of Buckfast bees in a field apiary at the Plateforme BioPark d'Archamps (Archamps, France). Emerging honey bees were placed in plastic cages (Ickowicz, France) and maintained in incubators at 33°C ± 1°C and 60% ±20% relative humidity. During the first day, the bees were fed syrup (InvertBee, Alp'Abeilles, France) *ad libitum*. 24 hours after emergence, the syrup was removed for 15 hours. Then, honey bees were placed individually in a homemade box and fed with 10µL of syrup supplied with *Nosema ceranae* spores (100,000 spores per bee). After consuming the solution, they were placed in a new collective box according to the experimental condition (control and inoculated bees). Sixteen days after inoculation, five control and three infected bees were collected and immediately subjected to the inclusion process. The infection was confirmed by microscopic observation of the gut contents of an inoculated bee. The sample preparation for MALDI IMS was identical to the one reported above **in section 3.1.2**.

4.2. Results and Discussion

Using the developed MALDI imaging approach, a total of 312 ions were recorded from the whole bee bodies within the mass range considered (**Figure 7**).

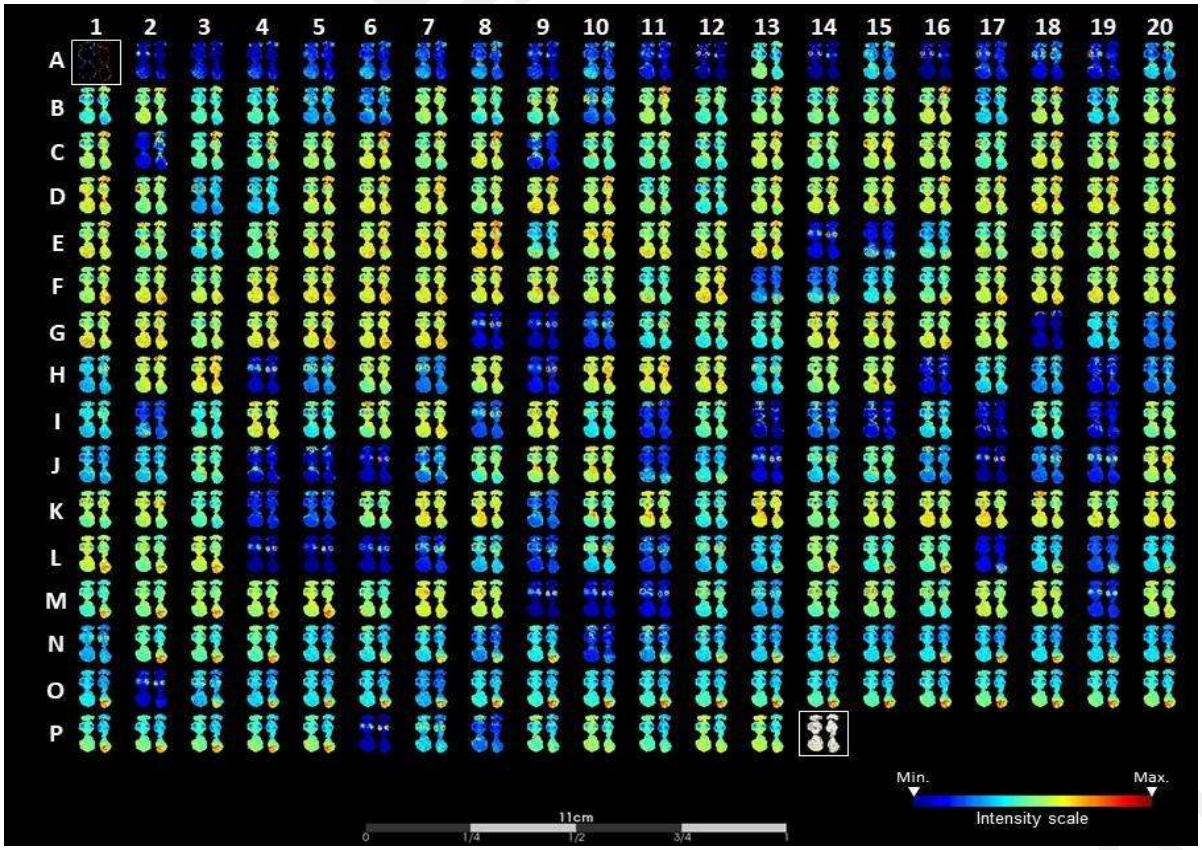

Figure 7: Tile view illustrating the molecular ions recorded from the whole bee bodies using MALDI imaging.

We first focused our analyses on the primary target of spores for development, the gut [53]. Principal component analysis (PCA) based on MALDI IMS spectra from control *versus* infected bees with *N. ceranae* revealed discriminative molecular patterns along with the three first components (**Figure 8A**).

To correlate these patterns with specific tissue locations, spectra were clustered and mapped using segmentation and each cluster was assigned a color and a specific molecular distribution throughout the bee body. As a result, clusters of spectra were found in the brain and the second thoracic ganglion, in the vertical flight muscle, and in the midgut (**Figure 8B**).

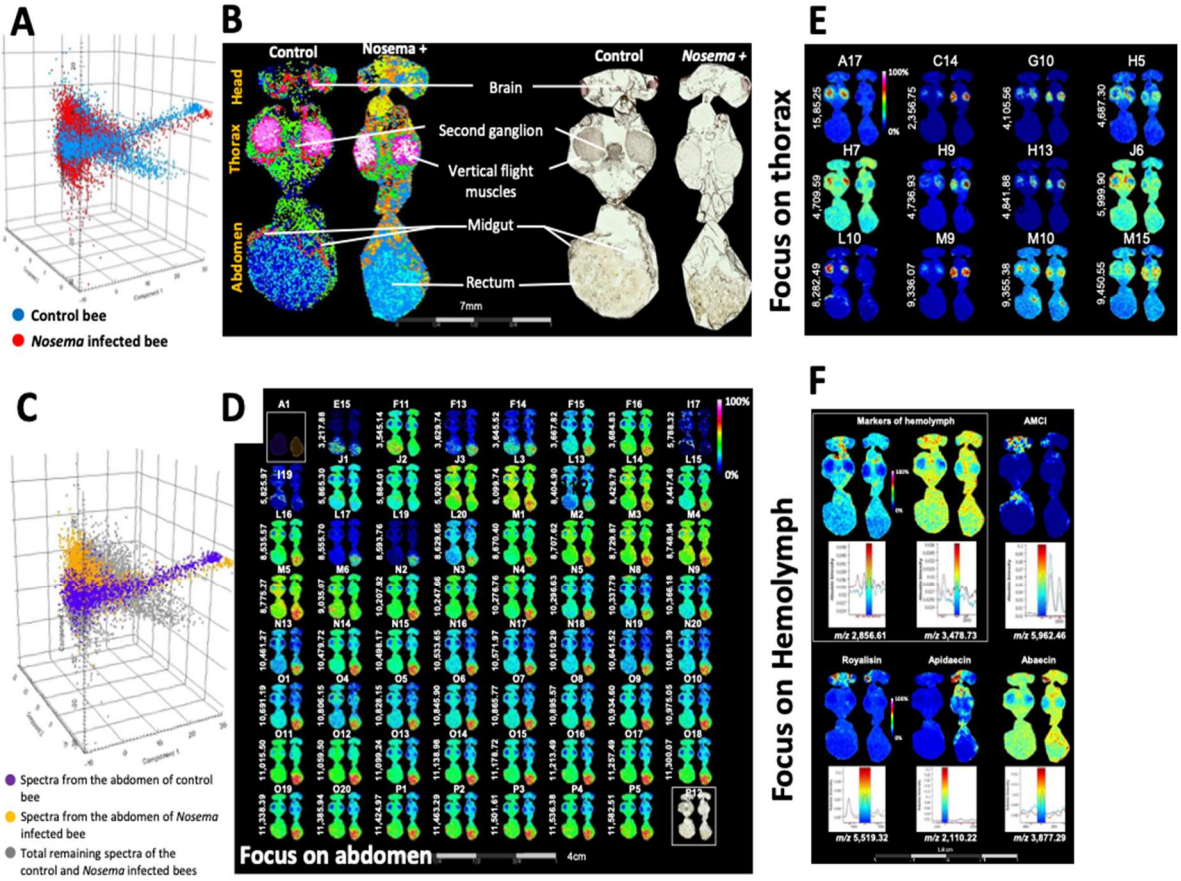

Figure 8: Unsupervised principal component analysis (A) and PCA-based molecular segmentation (B) of whole-body imaging spectra from control versus infected (*Nosema* +) honey bee by *Nosema ceranae*. Discriminant PCA (C) and differential ions patterns in abdomen (D) from *Nosema*- and *Nosema* + *A. mellifera*. Tile view of twelve differentially expressed molecular ions in the bees' thorax (E) following infection. Differential abundance intensities and mapping of characteristic markers expressed in the haemolymph (F), the hypopharyngeal gland and the thoracic muscles with respect to the histology and physiology of the honey bee.

We refined our analysis by extracting spectra from the abdomen of the control and *Nosema*-infected bees. Based on these spectra, the PCA revealed discriminative profiles (**Figure 8C)** and 62 differentially expressed molecular-related ions could be retrieved from the analysis (**Figure 8D**). First observations confirmed the results obtained with unsupervised hierarchical clustering, the distribution of the 62 molecular-related ions mapped two patterns in the abdomen, namely the midgut and the rectum. The molecular-related ions at *m/z* 5,788.32, 5,825.97, 5,884.01 and 5,920.61 were found to be more intense in the midgut of the control bee compared to the infected one (**Figure 8D**) whereas all the other molecular-related ions were distributed within the rectum and found to be more intense in the infected bees. *N. ceranae* spores are known to destroy epithelial cells of the midgut when multiplying. This phenomenon could explain why some proteins were less intense in infected bees. As for the rectum, we hypothesize that we observed some peptides/proteins of mature spores after being expelled from the midgut. To identify those potential markers of spores, complementary experiments will be necessary. Alteration of the gut microbiota by the infection could also explain a change in the proteomic profile of the gut [87].

Studying the molecular impact of nosemosis in the honey bee also implies looking beyond the local response in the abdomen. As demonstrated in this study, MALDI IMS allowed the recording of hundreds of ions throughout the honey bee body regardless of the unsupervised *vs* supervised strategy used. Indeed, the pathology associated with *N. ceranae* infection is already described in the literature [88] and different impacts were reported such as changes in metabolism [56] pheromone and hormone production [57], suppression of the immune function [55,59] or cognitive deficits [63]. All of these effects suggest an alteration of tissues involved in these deficient functions.
We used our MALDI IMS workflow to screen for all the differentially expressed signatures in the honey bee body and also noticed differential molecular patterns within the thorax (**Figure 8E**). Here again, three patterns of molecular distributions were observed. For the first one, molecular-related ions were found expressed in the vertical mass muscle with markers either over detected in the control (*m/z* 1,585.25, 4,709.59) or in the infected bee (*m/z* 2,356.75, 4,105.56, 4,736.93, 4,841.88, 9,336.07 and 9,450.55). Regarding the second pattern, molecular-related ions were also found in the vicinity of the vertical mass muscle and highly expressed in the control bee (*m/z* 4,687.30 and 5,999.90). Finally, the third pattern was represented by molecular ions depicted in the muscle and midgut epithelium only in the control condition (*m/z* 8,282.49) or for the molecular-related ions at *m/z* 9,355.38 in the muscle and the midgut content with equal distribution and intensity in both control and *Nosema* infection conditions. We hypothesize that the alteration of the muscles peptide/protein patterns could reflect the impact of *Nosema sp.* on flight abilities that is often observed in the natural environment [89] as the result of energetic stress caused by this disease [56]. To have a better understanding of the molecular impact of nosemosis on the honey bee, we will develop additional tissue-targeted bottom-up proteomics following the work of Houdelet and collaborators [67].

In order to pinpoint infection-related tissue markers, we naturally had a look at the systemic response in the haemolymph as a mirror of molecular changes following infections. To visualize the haemolymph distribution, we crossed the MALDI IMS (**Figure 8F**) and MALDI MFP (**Table 1**) datasets and matched up the two molecular-related ion *m/z* 2,856.61 and 3,478.73 (**Figure 8F**), which are not described in the scientific literature to the best of our knowledge. By this means, we could also assign the haemolymphatic distribution of the *Apis mellifera* chymotrypsin inhibitor (AMCI; theoretical molecular-related ions at *m/z* 5,962.46), which was observed intensely in the head and proximal section of the abdomen from the control bee. Interestingly, the distribution of the serine-protease inhibitor AMCI in the infected honey bee did not show such a similar and intense pattern (**Figure 8F**). The role of AMCI is still unclear but generally speaking, the serine protease type “chymotrypsin like” are involved in biological processes like digestion, coagulation, or cellular and humoral immunity [90]. Regarding the systemic inducible immune response, the three antimicrobial peptides (AMPs), Royalisin also known as defensin-1 (*m/z* 5,519.32), Apidaecin (*m/z* 2,110.22) and Abaecin (*m/z* 3,877.29), were retrieved from our MALDI IMS datasets. Royalisin was only mapped in the heads of both control and *Nosema*-infected bees with no evidence of differential profiles. This molecule is also associated with the hypopharyngeal glands, found in the head of bees. Unlike Apidaecin, which is located throughout the infected bee and only detected at a low level in the control bee, the haemolymphatic distribution of Abaecin was mainly in the head and between the midgut as well as the rectum, and was found to be more expressed in the infected bee. Many studies carried out on bees experimentally infected with *Nosema* spores have shown that the expression of the genes encoding AMPs was altered [55,59,91,92]. In their transcriptomic studies, Schwarz and Evans, also reported an increase expression of the *apidaecin* and *abaecin* genes seven days after inoculation of *N. ceranae* spores [93].

5. Concluding remarks

In honey bees, multiple stressors increase the risk of mortality by acting in concert on multifarious physiological pathways, resulting in alterations of tissue function. As in other animal models, mass spectrometry imaging approaches could be used to predict the impact of health stressors on the honey

bee. The present study is the first to offer a bimodal mass spectrometry methodology to assess the impact of *Nosema* spores on honey bee physiology. Our results clearly suggest that experimental infection with *Nosema* spores impacts the primary targeted gut tissues but also the haemolymph. The latter is the mirror of innate immunity but also and unexpectedly of the bee thoracic muscles. Overall, we found that combining MALDI MFP and MALDI IMS data is a powerful workflow in understanding and mapping the spatial changes that may occur during stress attacks.

6. Associated information

A manuscript presenting this work was published in *Proteomics* (open access). Citation recommendation: *Houdelet C, Sinpoo C, Chantaphanwattana T, Voisin SN, Bocquet M, Chantawannakul P, Bulet P. Proteomics of Anatomical Sections of the Gut of Nosema-Infected Western Honeybee (Apis mellifera) Reveals Different Early Responses to Nosema spp. Isolates. J Proteome Res. 2021 Jan 1;20(1):804-817. doi: 10.1021/acs.jproteome.0c00658. Epub 2020 Dec 11. PMID: 33305956.* The mass spectrometry proteomics data were deposited to the online open access repository Figshare with the following link 10.6084/m9.figshare.17311448.

7. Acknowledgements

The research leading to these results was funded by the European Union's Horizon 2020 research and innovation program, under grant agreement No 773921 (PoshBee). This work was supported by the EDCSV from University of Grenoble Alpes for the PhD allocation of Camille Houdelet. We would like to thank the Master 1 student François Di Franco, for the dissection and the MALDI MFPs.

8. References

1. Caprioli, R. M., Farmer, T. B., & Gile, J. (1997). Molecular Imaging of Biological Samples : Localization of Peptides and Proteins Using MALDI-TOF MS. *Analytical Chemistry*, *69*(23), 4751-4760. https://doi.org/10.1021/ac970888i

2. Karlsson, O., & Hanrieder, J. (2017). Imaging mass spectrometry in drug development and toxicology. *Archives of Toxicology*, *91*(6), 2283-2294. https://doi.org/10.1007/s00204-016-1905-6

3. Trim, P. J., & Snel, M. F. (2016). Small molecule MALDI MS imaging : Current technologies and future challenges. *Methods*, *104*, 127-141. https://doi.org/10.1016/j.ymeth.2016.01.011

4. Ly, A., Buck, A., Balluff, B., Sun, N., Gorzolka, K., Feuchtinger, A., Janssen, K.-P., Kuppen, P. J. K., van de Velde, C. J. H., Weirich, G., Erlmeier, F., Langer, R., Aubele, M., Zitzelsberger, H., McDonnell, L., Aichler, M., & Walch, A. (2016). High-mass-resolution MALDI mass spectrometry imaging of metabolites from formalin-fixed paraffin-embedded tissue. *Nature Protocols*, *11*(8), 1428-1443. https://doi.org/10.1038/nprot.2016.081

5. Dueñas, M. E., Essner, J. J., & Lee, Y. J. (2017). 3D MALDI Mass Spectrometry Imaging of a Single Cell : Spatial Mapping of Lipids in the Embryonic Development of Zebrafish. *Scientific Reports*, *7*(1), 14946. https://doi.org/10.1038/s41598-017-14949-x

6. Yalcin, E. B., & de la Monte, S. M. (2015). Review of Matrix-Assisted Laser Desorption Ionization-Imaging Mass Spectrometry for Lipid Biochemical Histopathology. *Journal of Histochemistry & Cytochemistry*, *63*(10), 762-771. https://doi.org/10.1369/0022155415596202

7. Goto-Inoue, N., Hayasaka, T., & Setou, M. (2010). Imaging Mass Spectrometry of Glycolipids. In *Methods in Enzymology* (Vol. 478, p. 287-301). Elsevier. https://doi.org/10.1016/S0076-6879(10)78014-9

8. Dilillo, M. (2017). Ultra-High Mass Resolution MALDI Imaging Mass Spectrometry of Proteins and Metabolites in a Mouse Model of Glioblastoma. *Scientific Reports*, *7*(1), 603. https://doi.org/10.1038/s41598-017-00703-w.

9. Llombart, V., Trejo, S. A., Bronsoms, S., Morancho, A., Feifei, M., Faura, J., García-Berrocoso, T., Simats, A., Rosell, A., Canals, F., Hernández-Guillamón, M., & Montaner, J. (2017). Profiling and identification of new proteins involved in brain ischemia using MALDI-imaging-mass-spectrometry. *Journal of Proteomics*, *152*, 243-253. https://doi.org/10.1016/j.jprot.2016.11.014

10. Ryan, D. J., Spraggins, J. M., & Caprioli, R. M. (2019). Protein identification strategies in MALDI imaging mass spectrometry : A brief review. *Current Opinion in Chemical Biology*, *48*, 64-72. https://doi.org/10.1016/j.cbpa.2018.10.023

11. Spraggins, J. M., Rizzo, D. G., Moore, J. L., Noto, M. J., Skaar, E. P., & Caprioli, R. M. (2016). Next-generation technologies for spatial proteomics : Integrating ultra-high speed MALDI-TOF and high mass resolution MALDI FTICR imaging mass spectrometry for protein analysis. *PROTEOMICS*, *16*(11-12), 1678-1689. https://doi.org/10.1002/pmic.201600003

12. Amstalden van Hove, E. R., Smith, D. F., & Heeren, R. M. A. (2010). A concise review of mass spectrometry imaging. *Journal of Chromatography A*, *1217*(25), 3946-3954. https://doi.org/10.1016/j.chroma.2010.01.033

13. Chaurand, P., Schwartz, S. A., & Caprioli, R. M. (2002). Imaging mass spectrometry : A new tool to investigate the spatial organization of peptides and proteins in mammalian tissue sections. *Current Opinion in Chemical Biology*, *6*(5), 676-681. https://doi.org/10.1016/S1367-5931(02)00370-8

14. Chaurand, P., Cornett, D. S., Angel, P. M., & Caprioli, R. M. (2011). *From Whole-body Sections Down to Cellular Level, Multiscale Imaging of Phospholipids by MALDI Mass Spectrometry*. *10*(2), O110.004259. https://doi.org/10.1074/mcp.O110.004259.

15. Han, C., Li, S., Yue, Q., Li, N., Yang, H., & Zhao, Z. (2019). Polydopamine-capped AgNPs as a novel matrix overcoming the ion suppression of phosphatidylcholine for MALDI MS comprehensive imaging of glycerophospholipids and sphingolipids in impact-induced injured brain. *The Analyst*, *144*(21), 6304-6312. https://doi.org/10.1039/c9an01361j

16. McDonnell, L. A., & Heeren, R. M. A. (2007). Imaging mass spectrometry. *Mass Spectrometry Reviews*, *26*(4), 606-643. https://doi.org/10.1002/mas.20124

17. Stoeckli, M., Chaurand, P., Hallahan, D. E., & Caprioli, R. M. (2001). Imaging mass spectrometry: A new technology for the analysis of protein expression in mammalian tissues. *Nature Medicine*, *7*(4), 493-496. https://doi.org/10.1038/86573

18. Buchberger, A. R., DeLaney, K., Johnson, J., & Li, L. (2017). Mass Spectrometry Imaging: A Review of Emerging Advancements and Future Insights. *Analytical Chemistry*, 57.

19. Carter, C. L., Jones, J. W., Farese, A. M., MacVittie, T. J., & Kane, M. A. (2016). Inflation-Fixation Method for Lipidomic Mapping of Lung Biopsies by Matrix Assisted Laser Desorption/Ionization–Mass Spectrometry Imaging. *Analytical Chemistry*, *88*(9), 4788-4794. https://doi.org/10.1021/acs.analchem.6b00165

20. Bunch, J., Clench, M. R., & Richards, D. S. (2004). Determination of pharmaceutical compounds in skin by imaging matrix-assisted laser desorption/ionisation mass spectrometry. *Rapid Communications in Mass Spectrometry*, *18*(24), 3051-3060. https://doi.org/10.1002/rcm.1725

21. Enthaler, B., Pruns, J. K., Wessel, S., Rapp, C., Fischer, M., & Wittern, K.-P. (2012). Improved sample preparation for MALDI–MSI of endogenous compounds in skin tissue sections and mapping of exogenous active compounds subsequent to ex-vivo skin penetration. *Analytical and Bioanalytical Chemistry*, *402*(3), 1159-1167. https://doi.org/10.1007/s00216-011-5562-6

22. Avery, J. L., McEwen, A., Flinders, B., Francese, S., & Clench, M. R. (2011). Matrix-assisted laser desorption mass spectrometry imaging for the examination of imipramine absorption by Straticell-RHE-EPI/001 an artificial model of the human epidermis. *Xenobiotica*, *41*(8), 735-742. https://doi.org/10.3109/00498254.2011.573015

23. Schulz, S., Becker, M., Groseclose, M. R., Schadt, S., & Hopf, C. (2019). Advanced MALDI mass spectrometry imaging in pharmaceutical research and drug development. *Current Opinion in Biotechnology*, *55*, 51-59. https://doi.org/10.1016/j.copbio.2018.08.003

24. Swales, J. G., Hamm, G., Clench, M. R., & Goodwin, R. J. A. (2018). Mass spectrometry imaging and its application in pharmaceutical research and development: A concise review. *International Journal of Mass Spectrometry*. *90*(10), 6051–6058. https://doi.org/10.1016/j.ijms.2018.02.007

25. Chumbley, C. W., Reyzer, M. L., Allen, J. L., Marriner, G. A., Via, L. E., Barry, C. E., & Caprioli, R. M. (2016). Absolute Quantitative MALDI Imaging Mass Spectrometry: A Case of Rifampicin in Liver Tissues. *Analytical Chemistry*, *88*(4), 2392-2398. https://doi.org/10.1021/acs.analchem.5b04409

26. Källback, P., Nilsson, A., Shariatgorji, M., & Andrén, P. E. (2016). MsIQuant – Quantitation Software for Mass Spectrometry Imaging Enabling Fast Access, Visualization, and Analysis of Large Data Sets. *Analytical Chemistry*, *88*(8), 4346-4353. https://doi.org/10.1021/acs.analchem.5b04603

27. Porta, T., Lesur, A., Varesio, E., & Hopfgartner, G. (2015). Quantification in MALDI-MS imaging: What can we learn from MALDI-selected reaction monitoring and what can we expect for imaging? *Analytical and Bioanalytical Chemistry*, *407*(8), 2177-2187. https://doi.org/10.1007/s00216-014-8315-5

28. Rzagalinski, I., & Volmer, D. A. (2017). Quantification of low molecular weight compounds by MALDI imaging mass spectrometry—A tutorial review. *Biochimica Et Biophysica Acta. Proteins and Proteomics*, *1865*(7), 726-739. https://doi.org/10.1016/j.bbapap.2016.12.011

29. Zhou, Q., Fülöp, A., & Hopf, C. (2020). Recent developments of novel matrices and on-tissue chemical derivatization reagents for MALDI-MSI. *Analytical and Bioanalytical Chemistry*. *413*(10), 2599–2617. https://doi.org/10.1007/s00216-020-03023-7

30. Boughton, B. A., & Thinagaran, D. (2018). Mass Spectrometry Imaging (MSI) for Plant Metabolomics. In C. António (Éd.), *Plant Metabolomics* (Vol. 1778, p. 241-252). Springer New York. https://doi.org/10.1007/978-1-4939-7819-9_17

31. Dong, Y., Li, B., Malitsky, S., Rogachev, I., Aharoni, A., Kaftan, F., Svatos, A., & Franceschi, P. (2016). Sample Preparation for Mass Spectrometry Imaging of Plant Tissues: A Review. *Front Plant Sci*, *7*, 60. https://doi.org/10.3389/fpls.2016.00060

32. Qin, L., Zhang, Y., Liu, Y., He, H., Han, M., Li, Y., Zeng, M., & Wang, X. (2018). Recent advances in matrix-assisted laser desorption/ionisation mass spectrometry imaging (MALDI-MSI) for *in situ*

analysis of endogenous molecules in plants. *Phytochemical Analysis*, *29*(4), 351-364. https://doi.org/10.1002/pca.2759

33. Susniak, K., Krysa, M., Gieroba, B., Komaniecka, I., & Sroka-Bartnicka, A. (2020). Recent developments of MALDI MSI application in plant tissues analysis. *Acta Biochimica Polonica*. *67*(3), 277–281. https://doi.org/10.18388/abp.2020_5394

34. Harris, A., Roseborough, A., Mor, R., Yeung, K. K.-C., & Whitehead, S. N. (2020). Ganglioside Detection from Formalin-Fixed Human Brain Tissue Utilizing MALDI Imaging Mass Spectrometry. *Journal of the American Society for Mass Spectrometry*, *31*(3), 479-487. https://doi.org/10.1021/jasms.9b00110

35. Seeley, E. H., & Caprioli, R. M. (2011). MALDI imaging mass spectrometry of human tissue: Method challenges and clinical perspectives. *Trends in Biotechnology*, *29*(3), 136-143. https://doi.org/10.1016/j.tibtech.2010.12.002

36. Verhaert, P. D., Conaway, M. C. P., Pekar, T. M., & Miller, K. (2007). Neuropeptide imaging on an LTQ with vMALDI source : The complete 'all-in-one' peptidome analysis. *International Journal of Mass Spectrometry*, *260*(2), 177-184. https://doi.org/10.1016/j.ijms.2006.11.008

37. Nunes, T. M., Mateus, S., Favaris, A. P., Amaral, M. F. Z. J., von Zuben, L. G., Clososki, G. C., Bento, J. M. S., Oldroyd, B. P., Silva, R., Zucchi, R., Silva, D. B., & Lopes, N. P. (2015). Queen signals in a stingless bee : Suppression of worker ovary activation and spatial distribution of active compounds. *Scientific Reports*, *4*(1), 7449. https://doi.org/10.1038/srep07449

38. Pratavieira, M., Menegasso, A. R. da S., Esteves, F. G., Sato, K. U., Malaspina, O., & Palma, M. S. (2018). MALDI Imaging Analysis of Neuropeptides in Africanized Honeybee (*Apis mellifera*) Brain: Effect of Aggressiveness. *Journal of Proteome Research*, *17*(7), 2358-2369. https://doi.org/10.1021/acs.jproteome.8b00098

39. Pratavieira, M., da Silva Menegasso, A. R., Garcia, A. M. C., dos Santos, D. S., Gomes, P. C., Malaspina, O., & Palma, M. S. (2014). MALDI Imaging Analysis of Neuropeptides in the Africanized Honeybee (*Apis mellifera*) Brain : Effect of Ontogeny. *Journal of Proteome Research*, *13*(6), 3054-3064. https://doi.org/10.1021/pr500224b

40. Catae, A. F., Roat, T. C., Oliveira, R. A. D., Nocelli, R. C. F., & Malaspina, O. (2014). Cytotoxic effects of thiamethoxam in the midgut and malpighian tubules of Africanized *Apis mellifera* (Hymenoptera : Apidae). *Microscopy Research and Technique*, *77*(4), 274-281. https://doi.org/10.1002/jemt.22339

41. Catae, A. F., da Silva Menegasso, A. R., Pratavieira, M., Palma, M. S., Malaspina, O., & Roat, T. C. (2018). MALDI-imaging analyses of honeybee brains exposed to a neonicotinoid insecticide : MALDI-imaging of honeybee brains. *Pest Management Science*, *75*(3), 607-615. https://doi.org/10.1002/ps.5226

42. Catae, A. F., Roat, T. C., Pratavieira, M., Silva Menegasso, A. R. D., Palma, M. S., & Malaspina, O. (2018). Exposure to a sublethal concentration of imidacloprid and the side effects on target and nontarget organs of Apis mellifera (Hymenoptera, Apidae). *Ecotoxicology*, *27*(2), 109-121. https://doi.org/10.1007/s10646-017-1874-4

43. Pratavieira, M., da Silva Menegasso, A. R., Roat, T., Malaspina, O., & Palma, M. S. (2020). In Situ Metabolomics of the Honeybee Brain : The Metabolism of l-Arginine through the Polyamine Pathway

in the Proboscis Extension Response (PER). *J Proteome Res*, *19*(2), 832-844. https://doi.org/10.1021/acs.jproteome.9b00653

44. Gallai, N., Salles, J.-M., Settele, J., & Vaissière, B. E. (2009). Economic valuation of the vulnerability of world agriculture confronted with pollinator decline. *Ecological Economics*, *68*(3), 810-821. https://doi.org/10.1016/j.ecolecon.2008.06.014

45. Baylis, K., Lichtenberg, E. M., & Lichtenberg, E. (2021). Economics of Pollination. *Annual Review of Resource Economics*, *13*(1), 101420-110406. https://doi.org/10.1146/annurev-resource-101420-110406

46. Kulhanek, K., Steinhauer, N., Rennich, K., Caron, D. M., Sagili, R. R., Pettis, J. S., Ellis, J. D., Wilson, M. E., Wilkes, J. T., Tarpy, D. R., Rose, R., Lee, K., Rangel, J., & vanEngelsdorp, D. (2017). A national survey of managed honey bee 2015–2016 annual colony losses in the USA. *Journal of Apicultural Research*, *56*(4), 328-340. https://doi.org/10.1080/00218839.2017.1344496

47. Potts, S. G., Biesmeijer, J. C., Kremen, C., Neumann, P., Schweiger, O., & Kunin, W. E. (2010). Global pollinator declines : Trends, impacts and drivers. *Trends in Ecology & Evolution*, *25*(6), 345-353. https://doi.org/10.1016/j.tree.2010.01.007

48. Goulson, D., Nicholls, E., Botias, C., & Rotheray, E. L. (2015). Bee declines driven by combined stress from parasites, pesticides, and lack of flowers. *Science*, *347*(6229), 1255957-1255957. https://doi.org/10.1126/science.1255957

49. O'Neal, S. T., Anderson, T. D., & Wu-Smart, J. Y. (2018). Interactions between pesticides and pathogen susceptibility in honey bees. *Current opinion in insect science*, *26*, 57-62.

50. Higes, M., Martín-Hernández, R., Botías, C., Bailón, E. G., González-Porto, A. V., Barrios, L., del Nozal, M. J., Bernal, J. L., Jiménez, J. J., Palencia, P. G., & Meana, A. (2008). How natural infection by *Nosema ceranae* causes honeybee colony collapse : Natural *Nosema ceranae* infection. *Environmental Microbiology*, *10*(10), 2659-2669. https://doi.org/10.1111/j.1462-2920.2008.01687.x

51. Staveley, J. P., Law, S. A., Fairbrother, A., & Menzie, C. A. (2014). A Causal Analysis of Observed Declines in Managed Honey Bees (*Apis mellifera*). *Human and Ecological Risk Assessment*, *20*(2), 566-591. https://doi.org/10.1080/10807039.2013.831263

52. Higes, M., Martín, R., & Meana, A. (2006). *Nosema ceranae*, a new microsporidian parasite in honeybees in Europe. *Journal of Invertebrate Pathology*, *92*(2), 93-95. https://doi.org/10.1016/j.jip.2006.02.005

53. Fries, I., Feng, F., da Silva, A., Slemenda, S. B., & Pieniazek, N. J. (1996). *Nosema ceranae* n. Sp. (Microspora, Nosematidae), morphological and molecular characterization of a microsporidian parasite of the Asian honey bee *Apis cerana* (Hymenoptera, Apidae). *European Journal of Protistology*, *32*(3), 356-365. https://doi.org/10.1016/S0932-4739(96)80059-9

54. Martín-Hernández, R., Bartolomé, C., Chejanovsky, N., Le Conte, Y., Dalmon, A., Dussaubat, C., García-Palencia, P., Meana, A., Pinto, M. A., Soroker, V., & Higes, M. (2018). *Nosema ceranae* in *Apis mellifera* : A 12 years postdetection perspective. *Environmental Microbiology*, *20*(4), 1302-1329. https://doi.org/10.1111/1462-2920.14103

55. Badaoui, B., Fougeroux, A., Petit, F., Anselmo, A., Gorni, C., Cucurachi, M., Cersini, A., Granato, A., Cardeti, G., Formato, G., Mutinelli, F., Giuffra, E., Williams, J. L., & Botti, S. (2017). RNA-sequence

analysis of gene expression from honeybees (*Apis mellifera*) infected with *Nosema ceranae*. *PloS ONE*, *12*(3), e0173438. https://doi.org/10.1371/journal.pone.0173438

56. Mayack, C., & Naug, D. (2009). Energetic stress in the honeybee *Apis mellifera* from *Nosema ceranae* infection. *Journal of Invertebrate Pathology*, *100*(3), 185-188. https://doi.org/10.1016/j.jip.2008.12.001

57. Mayack, C., Natsopoulou, M. E., & McMahon, D. P. (2015). *Nosema ceranae* alters a highly conserved hormonal stress pathway in honeybees : *Nosema ceranae* alters a hormonal pathway. *Insect Molecular Biology*, *24*(6), 662-670. https://doi.org/10.1111/imb.12190

58. Martín-Hernández, R., Higes, M., Sagastume, S., Juarranz, Á., Dias-Almeida, J., Budge, G. E., Meana, A., & Boonham, N. (2017). Microsporidia infection impacts the host cell's cycle and reduces host cell apoptosis. *PLoS ONE*, *12*(2), e0170183. https://doi.org/10.1371/journal.pone.0170183

59. Antúnez, K., Martín-Hernández, R., Prieto, L., Meana, A., Zunino, P., & Higes, M. (2009). Immune suppression in the honey bee (*Apis mellifera*) following infection by *Nosema ceranae* (Microsporidia). *Environmental Microbiology*, *11*(9), 2284-2290. https://doi.org/10.1111/j.1462-2920.2009.01953.x

60. Li, W., Evans, J. D., Li, J., Su, S., Hamilton, M., & Chen, Y. (2017). Spore load and immune response of honey bees naturally infected by *Nosema ceranae*. *Parasitology Research*, *116*(12), 3265-3274. https://doi.org/10.1007/s00436-017-5630-8

61. Huang, W.-F., Solter, L., Aronstein, K., & Huang, Z. (2015). Infectivity and virulence of *Nosema ceranae* and *Nosema apis* in commercially available North American honey bees. *Journal of Invertebrate Pathology*, *124*, 107-113. https://doi.org/10.1016/j.jip.2014.10.006

62. Roberts, K. E., & Hughes, W. O. (2014). Immunosenescence and resistance to parasite infection in the honey bee, *Apis mellifera*. *Journal of Invertebrate Pathology*, *121*, 1-6. https://doi.org/10.1016/j.jip.2014.06.004

63. Gage, S. L., Kramer, C., Calle, S., Carroll, M., Heien, M., & DeGrandi-Hoffman, G. (2017). *Nosema ceranae* parasitism impacts olfactory learning and memory and neurochemistry in honey bees (*Apis mellifera*). *Journal of Experimental Biology*, *221*(Pt 4), jeb161489. https://doi.org/10.1242/jeb.161489.

64. Goblirsch, M., Huang, Z. Y., & Spivak, M. (2013). Physiological and Behavioral Changes in Honey Bees (*Apis mellifera*) Induced by *Nosema ceranae* Infection. *PLoS ONE*, *8*(3), e58165. https://doi.org/10.1371/journal.pone.0058165

65. Li, H., Zhang, L., Ni, C., Shang, H., Zhuang, S., & Li, J. (2013). Molecular recognition of floral volatile with two olfactory related proteins in the Eastern honeybee (*Apis cerana*). *International Journal of Biological Macromolecules*, *56*, 114-121. https://doi.org/10.1016/j.ijbiomac.2013.01.032

66. Rubanov, A., Russell, K. A., Rothman, J. A., Nieh, J. C., & McFrederick, Q. S. (2019). Intensity of *Nosema ceranae* infection is associated with specific honey bee gut bacteria and weakly associated with gut microbiome structure. *Scientific Reports*, *9*(1), 1-8. https://doi.org/10.1038/s41598-019-40347-6

67. Houdelet, C. (s. d.). Proteomics of Anatomical Sections of the Gut of *Nosema*-Infected Western Honeybee (*Apis mellifera*) Reveals Different Early Responses to *Nosema* spp. Isolates. *Journal of Proteome Research*, 14.

68. Carreck, N. L., Andree, M., Brent, C. S., Cox-Foster, D., Dade, H. A., Ellis, J. D., Hatjina, F., & van Englesdorp, D. (2013). Standard methods for *Apis mellifera* anatomy and dissection. *Journal of Apicultural Research*, *52*(4), 1-40. https://doi.org/10.3896/IBRA.1.52.4.03

69. Arafah, K., Voisin, S. N., Masson, V., Alaux, C., Le Conte, Y., Bocquet, M., & Bulet, P. (2019). MALDI–MS Profiling to Address Honey Bee Health Status under Bacterial Challenge through Computational Modeling. *Proteomics*, *19*(23), e1900268. https://doi.org/10.1002/pmic.201900268

70. Croxatto, A., Prod'hom, G., & Greub, G. (2012). Applications of MALDI-TOF mass spectrometry in clinical diagnostic microbiology. *FEMS Microbiology Reviews*, *36*(2), 380-407. https://doi.org/10.1111/j.1574-6976.2011.00298.x

71. Boyer, P. H., Boulanger, N., Nebbak, A., Collin, E., Jaulhac, B., & Almeras, L. (2017). Assessment of MALDI-TOF MS biotyping for Borrelia burgdorferis sl detection in *Ixodes ricinus*. *PLOS ONE*, *12*(9), e0185430. https://doi.org/10.1371/journal.pone.0185430

72. Yssouf, A., Almeras, L., Terras, J., Socolovschi, C., Raoult, D., & Parola, P. (2015). Detection of *Rickettsia spp* in Ticks by MALDI-TOF MS. *PLOS Neglected Tropical Diseases*, *9*(2), e0003473. https://doi.org/10.1371/journal.pntd.0003473

73. Houdelet, C., Bocquet, M., & Bulet, P. (2020). MALDI Biotyping, an approach for deciphering and assessing the identity of the honeybee pathogen Nosema. *Rapid Communications in Mass Spectrometry: RCM*, *35*(3), e8980. https://doi.org/10.1002/rcm.8980

74. Zhang, Y., Chen, D., Du, M., Ma, L., Li, P., Qin, R., Yang, J., Yin, Z., Wu, X., & Xu, H. (2021). Insights into the degradation and toxicity difference mechanism of neonicotinoid pesticides in honeybees by mass spectrometry imaging. *Science of The Total Environment*, *774*, 145170. https://doi.org/10.1016/j.scitotenv.2021.145170

75. Fujino, Y., Minamizaki, T., Yoshioka, H., Okada, M., & Yoshiko, Y. (2016). Imaging and mapping of mouse bone using MALDI-imaging mass spectrometry. *Bone Reports*, *5*, 280-285. https://doi.org/10.1016/j.bonr.2016.09.004

76. Vandenbosch, M., Nauta, S. P., Svirkova, A., Poeze, M., Heeren, R. M. A., Siegel, T. P., Cuypers, E., & Marchetti-Deschmann, M. (2021). Sample preparation of bone tissue for MALDI-MSI for forensic and (pre)clinical applications. *Analytical and Bioanalytical Chemistry*, *413*(10), 2683-2694. https://doi.org/10.1007/s00216-020-02920-1

77. Li, B., Zhang, Y., Ge, J., Liu, K., & Li, P. (2018). Sample preparation for mass spectrometry imaging of leaf tissues : A case study on analyte delocalization. *Analytical and Bioanalytical Chemistry*, *410*(28), 7449-7456. https://doi.org/10.1007/s00216-018-1355-5

78. Chen, Y., Liu, Y., Allegood, J., Wang, E., Cachón-González, B., Cox, T. M., Merrill, A. H., & Sullards, M. C. (2010). Imaging MALDI Mass Spectrometry of Sphingolipids Using an Oscillating Capillary Nebulizer Matrix Application System. *Mass Spectrometry Imaging* (Vol. 656, p. 131-146). Humana Press. https://doi.org/10.1007/978-1-60761-746-4_7

79. Yang, E., Gamberi, C., & Chaurand, P. (2019). Mapping the fly Malpighian tubule lipidome by imaging mass spectrometry. *Journal of Mass Spectrometry*, *54*(6), 557-566. https://doi.org/10.1002/jms.4366

80. Schwartz, S. A., Reyzer, M. L., & Caprioli, R. M. (2003). Direct tissue analysis using matrix-assisted laser desorption/ionization mass spectrometry : Practical aspects of sample preparation. *Journal of Mass Spectrometry*, *38*(7), 699-708. https://doi.org/10.1002/jms.505

81. Norris, J. L., & Caprioli, R. M. (2013). Analysis of Tissue Specimens by Matrix-Assisted Laser Desorption/Ionization Imaging Mass Spectrometry in Biological and Clinical Research. *Chemical Reviews*, *113*(4), 2309-2342. https://doi.org/10.1021/cr3004295

82. Truong, J. X. M., Spotbeen, X., White, J., Swinnen, J. V., Butler, L. M., Snel, M. F., & Trim, P. J. (2021). Removal of optimal cutting temperature (O.C.T.) compound from embedded tissue for MALDI imaging of lipids. *Analytical and Bioanalytical Chemistry*, *413*(10), 2695-2708. https://doi.org/10.1007/s00216-020-03128-z

83. Lemaire, R., Wisztorski, M., Desmons, A., Tabet, J. C., Day, R., Salzet, M., & Fournier, I. (2006). MALDI-MS direct tissue analysis of proteins : Improving signal sensitivity using organic treatments. *Analytical chemistry*, *78*(20), 7145-7153.

84. Bania, J., Stachowiak, D., & Polanowski, A. (1999). Primary structure and properties of the cathepsin G/chymotrypsin inhibitor from the larval hemolymph of *Apis mellifera*. *European Journal of Biochemistry*, *262*(3), 680-687. https://doi.org/10.1046/j.1432-1327.1999.00406.x

85. Habermann, E. (1972). Bee and wasp venoms. *Science*, *177*(4046), 314-322. 10.1126/science.177.4046.314

86. Neumann, W., Habermann, E., & Amend, G. (1952). Zur papierelektrophoretischen fraktionierung tierischer gifte. *Naturwissenschaften*, *39*(12), 286-287. 10.1007/bf00591257

87. Paris, L., Peghaire, E., Moné, A., Diogon, M., Debroas, D., Delbac, F., & El Alaoui, H. (2020). Honeybee gut microbiota dysbiosis in pesticide/parasite co-exposures is mainly induced by *Nosema ceranae*. *Journal of Invertebrate Pathology*, *172*, 107348. https://doi.org/10.1016/j.jip.2020.107348

88. Dussaubat, C., Brunet, J.-L., Higes, M., Colbourne, J. K., Lopez, J., Choi, J.-H., Martín-Hernández, R., Botías, C., Cousin, M., McDonnell, C., Bonnet, M., Belzunces, L. P., Moritz, R. F. A., Le Conte, Y., & Alaux, C. (2012). Gut Pathology and Responses to the Microsporidium *Nosema ceranae* in the Honey Bee *Apis mellifera*. *PLoS ONE*, *7*(5), e37017. https://doi.org/10.1371/journal.pone.0037017

89. Kralj, J., & Fuchs, S. (2010). *Nosema sp.* influences flight behavior of infected honey bee (*Apis mellifera*) foragers. *Apidologie*, *41*(1), 21-28. https://doi.org/10.1051/apido/2009046

90. Veillard, F., Troxler, L., & Reichhart, J.-M. (2016). *Drosophila melanogaster* clip-domain serine proteases : Structure, function and regulation. *Biochimie*, *122*, 255-269. https://doi.org/10.1016/j.biochi.2015.10.007

91. Aufauvre, J., Misme-Aucouturier, B., Viguès, B., Texier, C., Delbac, F., & Blot, N. (2014). Transcriptome Analyses of the Honeybee Response to *Nosema* ceranae and Insecticides. *PLoS ONE*, *9*(3), e91686. https://doi.org/10.1371/journal.pone.0091686

92. Chaimanee, V., Chantawannakul, P., Chen, Y., Evans, J. D., & Pettis, J. S. (2012). Differential expression of immune genes of adult honey bee (*Apis mellifera*) after inoculated by *Nosema* ceranae. *Journal of Insect Physiology*, *58*(8), 1090-1095. https://doi.org/10.1016/j.jinsphys.2012.04.016

93. Schwarz, R. S., & Evans, J. D. (2013). Single and mixed-species trypanosome and microsporidia infections elicit distinct, ephemeral cellular and humoral immune responses in honey bees. *Developmental & Comparative Immunology*, *40*(3-4), 300-310. https://doi.org/10.1016/j.dci.2013.03